Zheng Li*, Miro Taphanel, Thomas Längle, and Jürgen Beyerer

Direct-imaging DOEs for high-NA multi-spot confocal surface measurement

Direct-imaging DOEs für konfokale Multi-Spot-Oberflächenmessung mit hoher NA

https://doi.org/10.1515/teme-2020-0103
Received December 31, 2020; accepted March 1, 2021

Abstract: Diffractive lens arrays with overlapping apertures can produce spot arrays with high numerical apertures (NAs). Combined with low-NA objectives, they can measure a large area with high lateral resolution. However, for surface measurements, the axial resolution of such setups is still fundamentally limited by the objectives. In this work, we propose a new design of diffractive optical elements (DOEs) to overcome this problem. The proposed Direct-imaging DOEs can perform 3D high-NA multi-spot surface measurements. Laterally, a non-vanishing contrast up to 1448 lp/mm is measured with a USAF resolution target. Axially, an average height of 917.5 nm with a standard deviation of 49.9 nm is measured with a calibrated step height target of 925.5 nm.

Keywords: DOE, diffractive optics, confocal microscopy, surface metrology.

Zusammenfassung: Diffraktive Linsenarrays mit überlappenden Aperturen können Spot-Arrays mit hohen numerischen Aperturen (NAs) erzeugen. Kombiniert mit Low-NA-Objektiven können sie einen großen Bereich mit hoher lateraler Auflösung messen. Für Oberflächenmessungen ist die axiale Auflösung solcher Aufbauten jedoch immer noch grundlegend durch die Objektive begrenzt. In dieser Arbeit schlagen wir ein neues Design von diffraktiven optischen Elementen (DOEs) vor, um dieses Problem zu lösen. Die vorgeschlagenen Direct-imaging DOEs können 3D-Multispot-Oberflächenmessungen mit hohen NA durchführen. Lateral wird ein nicht verschwindender Kontrast bis zu 1448 lp/mm mit einem USAF Auflösungstest gemessen. Axial wird eine durchschnittliche Höhe von 917.5 nm mit einer Standardabweichung von 49.9 nm bei einem kalibrierten Stufenhöhentarget von 925.5 nm gemessen.

Schlagwörter: DOE, diffraktive Optik, Konfokalmikroskop, Oberflächenmetrologie.

***Corresponding author: Zheng Li,** Vision and Fusion Laboratory (IES), Karlsruhe Institute of Technology (KIT), Karlsruhe, Germany; and Fraunhofer Institute of Optronics, System Technologies and Image Exploitation (IOSB), Karlsruhe, Germany, e-mail: zheng.li@iosb.fraunhofer.de
Miro Taphanel, Jürgen Beyerer, Vision and Fusion Laboratory (IES), Karlsruhe Institute of Technology (KIT), Karlsruhe, Germany; and Fraunhofer Institute of Optronics, System Technologies and Image Exploitation (IOSB), Karlsruhe, Germany
Thomas Längle, Fraunhofer Institute of Optronics, System Technologies and Image Exploitation (IOSB), Karlsruhe, Germany

1 Introduction

There is an unavoidable trade-off between resolution and field-of-views (FOVs) in traditional confocal microscopy. The magnifications of objectives usually increase with their NAs, which limit their FOVs. Although high-NA objectives with large FOVs such as lithography lenses exist, they are very expensive and difficult to produce, which makes them impractical for microscopy applications [23].

In the previous research, different kinds of array illuminators are proposed to solve the problem [22, 5, 10, 11, 1, 12, 17, 16]. They can produce focused spots over a large area and measure large samples by scanning. Among them, illuminators based on micro lens arrays [10, 11] and the Talbot effect [12, 17] are limited in resolution. It is difficult for them to achieve high NAs due to aberrations and diffraction in the Fresnel regime. In contrast to the traditional micro-lens arrays, diffractive lens arrays with overlapping apertures release the restriction between the pitches and the NAs of the micro lenses. They can overcome the limitation between resolution and FOVs of microscope objectives, and produce high-NA spots in a dense grid [5, 16]. Such DOEs are first used as pure illuminators in transmission microscopes, and later adapted into reflective microscopes after modifications [6, 8]. The proposed microscope setups can keep large FOVs of the low-NA objectives while maintaining the same lateral resolution as high-NA objectives. For example, Stenau et al. [16] have demonstrated a diffractive lens array with a pitch of 44 µm and an NA of 0.48, and reported a lateral non-vanishing contrast of 900 lp/mm with a 4× 0.32 NA objective in the experiment.

However, for surface topography measurement with the diffractive lens arrays in previous research [5, 16, 9],

although the lateral resolution can be improved by the high-NA diffractive lens arrays, the axial resolution is still fundamentally limited by the low-NA objectives in theory [6, 21]. To overcome such limitation and increase the axial resolution, Direct-imaging DOEs are proposed in this work. They act exactly as finite-conjugate high-NA objectives and can perform 3D multi-spot confocal surface measurements with high resolution, which solve the problem of previous diffractive lens arrays. The proposed DOEs are designed by superposition of field distributions of different lenses, and then overlapped to form an array. The size of the array can be expanded to cover a large measurement area. Besides, the DOEs can be easily replicated by mass production with lithography to reduce the cost. In the following sections, the design procedures of the Direct-imaging DOEs are introduced. Experiments with a USAF resolution target and a step height target are demonstrated to show the capabilities of the proposed DOEs for high-resolution measurement in both lateral and axial directions.

We note that a shorter conference version of this paper appeared in [7]. Our previous conference paper does not cover all the details of the design process and it also lacks experiments for axial surface height measurements. This manuscript introduces the detailed design procedures and demonstrates axial measurements of standard step height target by the proposed DOEs.

2 Design and simulation

The design of the DOEs begins with construction of a unit element. The unit element is composed of two field distributions of two diffractive lenses. One focuses plane-wave illumination to a spot. The other one images the produced spot back to an intermediate image, which is shown in Figure 1. By the principle of the multi-functional DOEs [2], the two lenses can function at the same time by simply adding their field distributions together.

The field distribution u_1 of the illumination lens is formed by propagation of the designed focused spot pattern u_{spot} after a certain working distance d. Rayleigh-Sommerfeld integral [14, 15, 13] is chosen as the diffraction propagation method, which is expressed as

$$u_1(\mathbf{r}) = \mathcal{RS}(u_{\text{spot}}, d) = \iint_{\Sigma} u_{\text{spot}}(\mathbf{r}') \frac{e^{-ik|\mathbf{r}-\mathbf{r}'|}d}{|\mathbf{r}-\mathbf{r}'|^2} \mathrm{d}x'\mathrm{d}y', \quad (1)$$

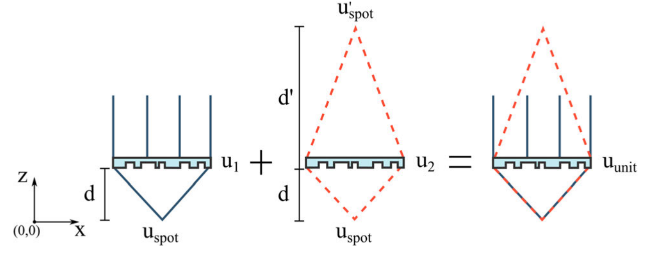

Figure 1: Design of the unit element by superposition of two field distributions.

where $k = 2\pi/\lambda$ is the wavenumber, λ is the wavelength, $\mathbf{r} = (x, y, z)$ is the coordinate on the DOE plane at $z = d$ if we assume the plane of u_{spot} is at $z = 0$ in Figure 1, Σ denotes the surface on the boundary, i. e. the plane of u_{spot} and the semi-infinite sphere above it, $\mathbf{r}' = (x', y', z')$ is the coordinate on Σ. In this work, u_{spot} is the theoretical field distribution of the Airy disc, which is expressed as

$$u_{\text{spot}}(\mathbf{r}) = \frac{2J_1(k\text{NA}|\mathbf{r}|)}{k\text{NA}|\mathbf{r}|}, \quad (2)$$

where J_1 represent Bessel function of the first kind and order, k is the wavenumber, and NA is the designed numerical aperture.

Similarly, the field distribution u_2 of the imaging lens can be calculated as

$$u_2(\mathbf{r}) = \frac{\mathcal{RS}(u'_{\text{spot}}, d')^*}{\mathcal{RS}(u_{\text{spot}}, d)}, \quad (3)$$

where u'_{spot} is the designed intermediate spot which can also be represented by Equation (2) with a different numerical aperture NA$'$, and d' is the designed distance from the DOE plane to the intermediate image shown in Figure 1. The complex conjugate is necessary to reverse the wave propagation direction.

Therefore, the field distribution u_{unit} of the unit element can be easily calculated by

$$u_{\text{unit}}(\mathbf{r}) = u_1(\mathbf{r}) + Wu_2(\mathbf{r}), \quad (4)$$

where W is a constant ratio which needs to be optimized later.

By the above-mentioned process, the calculated unit element can produce a focused spot by plane-wave illumination and then image the spot back to the intermediate plane by itself. Afterwards, the final DOE phase pattern is calculated as Figure 2 shows. First, in order to create a spot array, the unit element is replicated and overlapped with a certain lateral pitch. When z is set at the plane of the DOEs

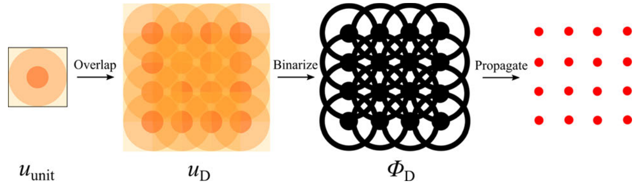

Figure 2: Design process of the Direct-imaging DOEs [8]. The unit field distribution u_{unit} is replicated, laterally shifted and overlapped, which results in the field distribution u_D. ϕ_D is the phase of the field distribution u_D after binarization. The result is a spot array after propagation through the working distance.

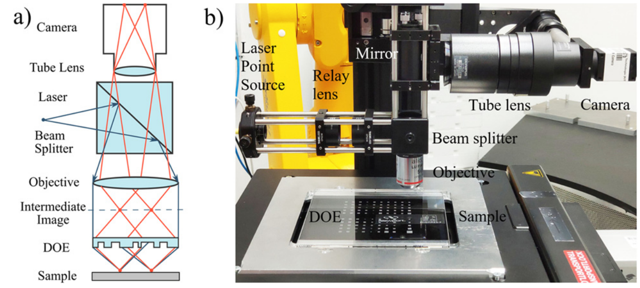

Figure 3: (a) Schematic of the DOE-based confocal microscope setup. (b) Photo of the measurement setup.

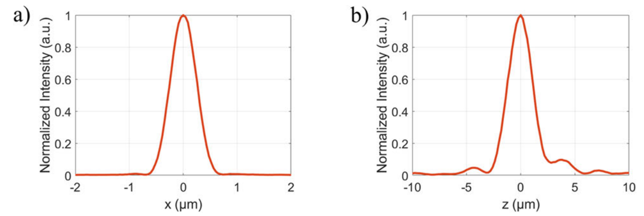

Figure 4: Size of the produced central spot in the 5×5 spot array with 100 μm pitch. (a) Lateral size of the spot, FWHM = 0.57 μm. (b) Axial size of the spot, FWHM = 2.61 μm.

($z = d$), the total field distribution u_D can thus be calculated by the following equation

$$u_D(x,y) = \sum_{i,j} u_{unit}(x + ip, y + jp), \quad (5)$$

where p is the designed pitch and i, j are the numbers of spots in the array in x and y directions respectively.

Second, the phase of the field distribution is extracted and binarized as the following equation shows

$$\phi_D = \text{mod}\left(\left\lfloor \frac{\arg(u_D) + B}{\pi} \right\rfloor, 2\right)\pi, \quad (6)$$

where mod is the modulo function and B is a constant binarization factor. Afterwards, the binarized phase pattern ϕ_D can again be examined by diffraction simulation with Rayleigh-Sommerfeld integral. The image of the spots on the intermediate plane can be obtained by simulation and thus a signal-to-background ratio of the spots can be easily defined and calculated. The parameters such as W and B are set as zero at first, and then they are optimized iteratively by the gradient descent algorithm in the simulation to maximize the signal-to-background ratio in the intermediate image.

By the above-mentioned process, the proposed Direct-imaging DOEs with different number of spots, pitches and working distances are designed. The DOEs are designed for the wavelength of 785 nm. Later, a binary phase mask is produced by e-beam lithography in Fraunhofer IOF (Institute for Applied Optics and Precision Engineering) according to the described design process. The DOE prototype is tested in experiments and the results are shown in the following sections.

3 Experiment results

3.1 Spot size measurement

For testing the DOE prototype, an experiment setup is built, which is shown in Figure 3. A laser beam of a wavelength of 785 nm is emitted by a fiber-coupled diode laser with a power of 10 mW, reflected by a beam splitter and then collimated by a 5× 0.15 NA objective. The collimated plane wave illuminates the DOEs, which focus the illumination into a spot array. The DOE prototype has a minimum feature size of 400 nm.

In the first experiment, the spot size is measured. A 100× 0.9 NA objective, a 0.63× tube lens and another camera with a pixel size of 6.5 μm are put under the DOE, which measures the produced spots by axial scanning. Figure 4 shows the measured central spot size of a 5×5 array with a pitch of 100 μm produced by a DOE pattern. It has a designed working distance d of 1 mm, a distance to the intermediate image d' of 16 mm and a simulated NA of 0.7. The lateral full width at half maximum (FWHM) of the central spot is 0.57 μm and the axial FWHM is 2.61 μm. The slight asymmetry in the axial response is mainly due to the imperfection of the collimated laser beam, which is slightly diverging in this case. It roughly corresponds to an NA of 0.68, which is calculated by the following equation [20]:

$$\text{AFWHM} = 0.89 \frac{\lambda}{n - \sqrt{n^2 - \text{NA}^2}}, \quad (7)$$

where AFWHM is the measured axial FWHM and n is the refractive index.

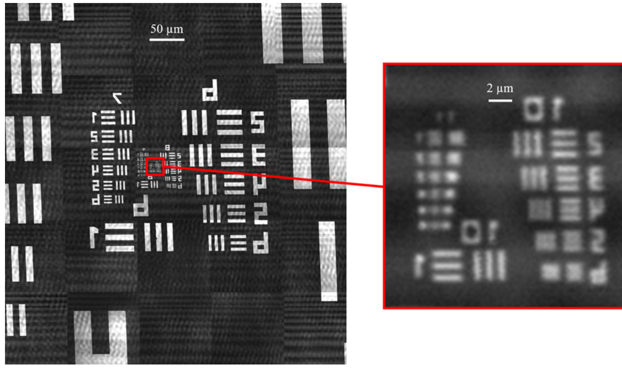

Figure 5: Confocal scanning image of the resolution target by a Direct-imaging DOE with 5×5 100 µm pitch spot array and a 5× 0.15 NA objective.

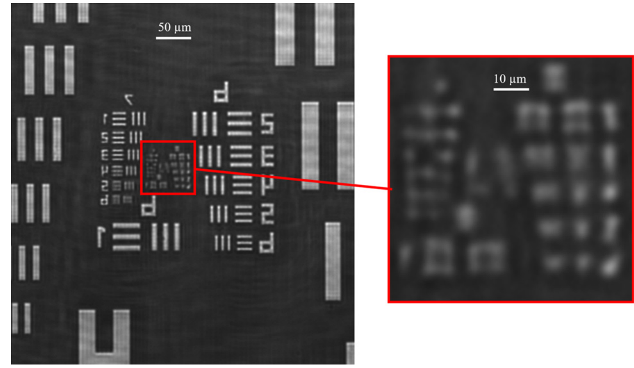

Figure 6: Wide-field image of the resolution target by a 5× 0.15 NA objective.

3.2 Lateral measurement

Afterwards, in order to test the lateral resolution of the proposed DOE-based confocal setup in Figure 3, a high-resolution USAF test target from Newport is placed underneath with a finest stripe of 3649 lp/mm. The illumination spots produced by the DOE are imaged by itself to an intermediate image. Then the intermediate image is imaged by a 5× objective and a 1× tube lens onto the camera sensor in Figure 3, which has a pixel size of 4.5 µm. In such a configuration, the DOE acts exactly as a high-NA finite-conjugate objective and it can provide high resolution in both lateral and axial directions for surface topography measurement.

The resolution target is placed on the focal plane of the DOE. It is moved and scanned laterally by a piezo stage with a scanning step of 0.2 µm and a camera frame rate of 100 fps. The imaging system takes images of the 5×5 intermediate spot array reflected by the target. For each spot, the central pixel is used as the pinhole and the intensity is recorded at every scanning step. The pixels are simply aligned after the measurement to reconstruct the scanning confocal image. The result is shown in Figure 5. Some stitching artifacts and inclination can be observed in the image due to the non-orthogonality of the two axes of the piezo stage. There are also stripes due to power drifting of the laser and interference with the stray light. Nevertheless, the finest line pairs which can still be clearly distinguished is in group 10 number 4, which corresponds to a spatial frequency of 1448 lp/mm. Compared to the wide-field image in Figure 6 which is taken by the 5× objective alone, the DOE significantly increases the lateral resolution of the low-NA objective.

3.3 Axial measurement

Next, a plane mirror is placed under the DOEs. It is scanned by the piezo stage axially. The intensity of the intermediate spots is again recorded to test the axial response of the setup for surface measurement. Figure 7(a) shows the confocal axial response of the central spot in the same 5×5 spot array with 100 µm pitch. An axial FWHM of 2.24 µm is measured.

However, if the number of spots increases, the signal will become noisy due to cross talks among the micro lenses in the DOEs [6]. There are several kinds of cross talks. On the one hand, for a single unit element, when the illumination lens projects the spots, the imaging lens also produces an out-of-focus spot around the original one. The blurred spot will become noise in the intermediate image. On the other hand, the spot produced by the unit element will not only be imaged by itself, but also be imaged by the adjacent elements and eventually it will overlap with the adjacent spots in the intermediate image. Besides, a binary DOE pattern has a diffraction efficiency lower than 50 percent in theory [18]. Other diffraction orders also enter the imaging system and become part of the background noise. Thus, further increase of the number of spots reduces the

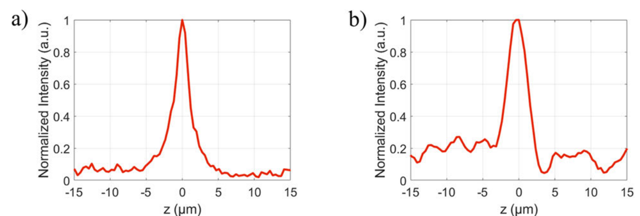

Figure 7: Confocal axial response of a plane mirror. (a) Central spot in the 5×5 spot array with 0.68 NA and 100 µm pitch, FWHM = 2.24 µm. (b) Central spot in the 25×25 spot array with 0.5 NA and 200 µm pitch, FWHM = 3.46 µm.

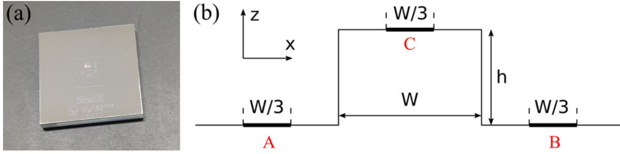

Figure 8: VLSI SHS-9400QC step height standard calibration target. (a) Picture of the target. (b) Cross section of the measurement area.

signal-to-noise ratio and the spots in the intermediate image might become indistinguishable [8].

Changing the spot arrangement, for example, into a line, increasing the pitch of the array, or decreasing the NAs of the DOEs can reduce the cross-talk. For example, the axial response of the central spot in a 25×25 spot array with 0.5 NA and 200 µm pitch is measured as Figure 7(b) shows. It appears that with a larger pitch the spot can still be distinguished in such a large grid.

Furthermore, a VLSI SHS-9400QC traceable step height standard target is tested by the setup to examine its measurement uncertainty. The target is a piece of quartz with chromium coating, which has a precisely etched convex bar with a width of 100 µm and a certified height of 925.5 ± 5.4 nm as shown in Figure 8. The height of the bar is measured according to the measurement procedures of VLSI [19, 3], which are introduced as follows. Along the cross section of the certified region of the target, three lines are measured, which are noted as A, B and C in Figure 8b. The length of each line is 33 µm, which is a third of the width of the bar on the step height target. The target is scanned axially to measure the height in these regions by 3 adjacent spots in the 5×5 spot array produced by the DOE in the above-mentioned setup. Each line is sampled with a step of 3 µm in x direction in Figure 8. Then, the 3 lines in Figure 8 can be fitted by the following equation [4] as

$$z = \begin{cases} ax + b_1, & x \in (A, B), \\ ax + b_2, & \text{otherwise}, \end{cases} \tag{8}$$

where z is the measured height, x is the lateral position and a, b_1 and b_2 are the line fitting parameters. Thus the height of the bar h can be derived as

$$h = \frac{b_2 - b_1}{\sqrt{a^2 + 1}}. \tag{9}$$

The process is repeated 10 times with a step of 10 µm in y direction along the bar. Afterwards, the lines at each y position are fitted and the height of the bar is calculated. The measurement results have a mean value of 917.5 nm with a standard deviation of 49.9 nm, which is close to the ground truth value. The measurement error mainly comes from the image noise by the stray light, which is mainly composed of 3 parts. First, there is considerable reflection from the objective because its coating is not designed for the near-infrared wavelength. Second, there is more than half of the energy in the unwanted diffraction orders because of the limited diffraction efficiency of the binary phase mask. Third, the Direct-imaging DOE introduces certain amount of disturbances itself like cross talks in traditional micro-lens arrays, which is also described in the previous sections. The noise and measurement uncertainty can hopefully be reduced by changing the objective coating, using a multi-level phase mask to increase the diffraction efficiency or changing the spot arrangement.

4 Conclusion

There is a trade-off between resolution and FOVs of microscope objectives. In previous research, diffractive lens arrays with overlapping apertures are used to replace high-NA objectives in confocal microscopy to increase the FOVs and reduce the cost while maintaining the high lateral resolution. However, in opaque surface measurement, the axial resolution of such setups is still fundamentally limited by the imaging objectives. In this work, the Direct-imaging DOEs are proposed to overcome this limit and to increase the axial resolution of the previous diffractive lens arrays for opaque surface measurements. The proposed DOEs utilize the idea of superposition to create multi-functional DOEs. The resultant DOEs can not only project spot arrays with high numerical apertures but also image the spots back to an intermediate plane. They have the same lateral and axial discerning capabilities as traditional high-NA objectives.

The DOEs are designed by Rayleigh-Sommerfeld integral under scalar approximation of Maxwell's equations. A prototype of the DOEs is produced. A DOE-based confocal microscope setup is build to test the prototype. Experiments show that spots with NA = 0.68 are produced by the DOEs, which is close to the designed NA of 0.7. A USAF resolution target is measured. The setup demonstrates a spatial cut-off frequency of 1448 lp/mm. And a confocal axial response by a plane mirror with a FWHM of 2.24 µm is measured. Furthermore, a step height standard target with a certified height of 925.5 nm is used to test the axial measurement uncertainty of the setup. The measured heights have a mean value of 917.5 nm with a standard deviation of 49.9 nm. However, the images still suffer from disturbances by stray light, especially when the number

of spots in the array increases. The stray light leads to a lower signal-to-noise ratio and a larger measurement uncertainty. By simulation, 1D arrangement of the spots or a larger pitch can reduce the disturbances and the setup can be used as a line scanning device [6].

In the future, application of the DOEs in fluorescence microscopy for high-resolution large-area measurement will be investigated, which will largely improve the stray light problem with the help of emission filters. Furthermore, new possibilities to combine the DOEs with structured illumination and interference will also be explored.

References

1. K. Brenner, T. Stenau and M. Azizian. Entwicklung eines scannenden Mikroskops mit diffraktiven Mikrolinsen. In *Online-Zeitschrift der Deutschen Gesellschaft für angewandte Optik e. V.*, Braunschweig, May 2013.
2. E. Dai, C. Zhou, P. Xi and L. Liu. Multifunctional double-layered diffractive optical element. *Optics Letters*, 28 (17): 1513–1515, 2003.
3. P. de Groot and D. Fitzgerald. Measurement, certification and use of step-height calibration specimens in optical metrology. In P. Lehmann, W. Osten and A. Albertazzi Gonçalves, Jr., editors, *Optical Measurement Systems for Industrial Inspection X*, Volume 10329, pp. 328–336. International Society for Optics and Photonics, SPIE, 2017. 10.1117/12.2269800.
4. A. Forbes, P. Harris and R. K. Leach. The comparison of algorithm for the assessment of type a1 surface texture reference artefacts. Technical Report CMSC 33/03, National Physical Laboratory, 2018.
5. B. Hulsken, D. Vossen and S. Stallinga. High NA diffractive array illuminators and application in a multi-spot scanning microscope. *Journal of the European Optical Society – Rapid Publications*, 7, 2012.
6. Z. Li. Application of diffractive optical elements in confocal microscopy. In M. Taphanel and J. Beyerer, editors, *Proceedings of the 2018 Joint Workshop of Fraunhofer IOSB and Institute for Anthropomatics, Vision and Fusion Laboratory*. KIT Scientific Publishing, Karlsruhe, 2019.
7. Z. Li, M. Taphanel, T. Längle and J. Beyerer. Direct-imaging DOEs for high-NA multi-spot confocal microscopy. *tm - Technisches Messen*, 87 (s1): s40–s43, 01 Sep. 2020. 10.1515/teme-2020-0017.
8. Z. Li, M. Taphanel, T. Längle and J. Beyerer. Application of DOE in confocal microscopy for surface measurement. In M. Rosenberger, P.-G. Dittrich and B. Zagar, editors, *IMEKO Joint TC1–TC2 International Symposium on Photonics and Education in Measurement Science*, Volume 11144, pp. 254–261. International Society for Optics and Photonics, SPIE, 2019.
9. X. Liu and K.-H. Brenner. High resolution wavefront measurement with phase retrieval using a diffractive overlapping micro lens array. In W. Osten, editor, *Fringe 2013*, pp. 233–236. Springer Berlin Heidelberg, Berlin, Heidelberg, 2014. ISBN 978-3-642-36359-7.
10. A. Orth and K. Crozier. Microscopy with microlens arrays: high throughput, high resolution and light-field imaging. *Opt. Express*, 20 (12): 13522–13531, Jun 2012. 10.1364/OE.20.013522.
11. A. Orth and K. B. Crozier. High throughput multichannel fluorescence microscopy with microlens arrays. *Opt. Express*, 22 (15): 18101–18112, Jul 2014. 10.1364/OE.22.018101.
12. S. Pang, C. Han, J. Erath, A. Rodriguez and C. Yang. Wide field-of-view Talbot grid-based microscopy for multicolor fluorescence imaging. *Opt. Express*, 21 (12): 14555–14565, Jun 2013. 10.1364/OE.21.014555.
13. F. Shen and A. Wang. Fast-Fourier-Transform based numerical integration method for the Rayleigh-Sommerfeld diffraction formula. *Applied Optics*, 45 (6): 1102–1110, 2006.
14. A. Sommerfeld. Mathematische Theorie der Diffraction. *Mathematische Annalen*, 47 (2): 317–374, 1896.
15. A. Sommerfeld. *Mathematical Theory of Diffraction*. Birkhäuser Boston, Boston, MA, 2004. ISBN 978-0-8176-8196-8. 10.1007/978-0-8176-8196-8_2.
16. T. Stenau and K.-H. Brenner. Diffractive lenses with overlapping aperture a new tool in scanning microscopy. In *Imaging Systems and Applications*, p. IT1F–1. Optical Society of America, 2016.
17. Y. Sun and S. Pang. Multi-perspective scanning microscope based on Talbot effect. *Applied Physics Letters*, 108 (2): 021102, 2016.
18. G. J. Swanson. Binary optics technology: the theory and design of multi-level diffractive optical elements. Technical report, Lincoln Laboratory, Massachusetts Institute of Technology, 1989.
19. VLSI Standards. Application note: Step height standards for use with KLA-Tencor instruments, 2010. Rev.AB.
20. T. Wilson. Resolution and optical sectioning in the confocal microscope. *Journal of Microscopy*, 244 (2): 113–121, 2011.
21. T. Wilson and C. Sheppard. *Theory and Practice of Scanning Optical Microscopy*, Volume 180. Academic Press London, 1984.
22. J. Wu, X. Cui, G. Zheng, Y. M. Wang, L. M. Lee and C. Yang. Wide field-of-view microscope based on holographic focus grid illumination. *Opt. Lett.*, 35 (13): 2188–2190, Jul 2010. 10.1364/OL.35.002188.
23. G. Zheng. *Fourier Ptychographic Imaging: A Matlab Tutorial*. Morgan & Claypool Publishers, 2016.

Bionotes

Zheng Li
Vision and Fusion Laboratory (IES), Karlsruhe Institute of Technology (KIT), Karlsruhe, Germany
Fraunhofer Institute of Optronics, System Technologies and Image Exploitation (IOSB), Karlsruhe, Germany
zheng.li@iosb.fraunhofer.de

Zheng Li received his Master's degree from Karlsruhe School of Optics & Photonics (KSOP) at Karlsruhe Institute of Technology (KIT) in 2016 and his Bachelor's degree from School of Mechanical Engineering at Shanghai Jiao Tong University (SJTU) in 2013. Since September 2016, he has joined Vision and Fusion Laboratory (IES) as a doctor candidate. His research interests include electromagnetic simulation, diffractive optics and microscopy.

Miro Taphanel
Vision and Fusion Laboratory (IES), Karlsruhe Institute of Technology (KIT), Karlsruhe, Germany
Fraunhofer Institute of Optronics, System Technologies and Image Exploitation (IOSB), Karlsruhe, Germany
miro@gixel.de

Miro Taphanel studied mechanical engineering at the University of Karlsruhe and received his diploma with distinction in 2010. He received his doctor degree in Vision and Fusion Laboratory (IES). His field of work is optical metrology for dimensional and material sensing tasks. The work takes place in close cooperation with the Department of Visual Inspection Systems (SPR) at Fraunhofer IOSB in Karlsruhe. Currently he serves as the CEO of Gixel GmbH.

Thomas Längle
Fraunhofer Institute of Optronics, System Technologies and Image Exploitation (IOSB), Karlsruhe, Germany
thomas.laengle@iosb.fraunhofer.de

Thomas Längle is adjunct professor at Karlsruhe Institute of Technology (KIT) and the head of the business unit "Vision Based Inspection Systems" (SPR) at Fraunhofer IOSB in Karlsruhe, Germany. His research interests included different aspects of image processing and real-time algorithms for inspection systems.

Jürgen Beyerer
Vision and Fusion Laboratory (IES), Karlsruhe Institute of Technology (KIT), Karlsruhe, Germany
Fraunhofer Institute of Optronics, System Technologies and Image Exploitation (IOSB), Karlsruhe, Germany
juergen.beyerer@iosb.fraunhofer.de

Jürgen Beyerer has been a full professor for informatics at the Institute for Anthropomatics and Robotics at the Karlsruhe Institute of Technology (KIT) since March 2004 and director of the Fraunhofer Institute of Optronics, System Technologies and Image Exploitation (IOSB) in Ettlingen, Karlsruhe, Ilmenau, Lemgo and Görlitz. He is Spokesman of the Fraunhofer Group for Defense and Security VVS and he is member of acatech, National Academy of Science and Engineering. Furthermore, he is Head of team 7 of the platform "Lernende Systeme" and Spokesman of the Competence Center Robotic Systems for Decontamination in Hazardous Environments (ROBDEKON). Research interests include automated visual inspection, signal and image processing, pattern recognition, metrology, information theory, machine learning, system theory security, autonomous systems and automation.